Secreted Biomolecules Alter the Biological Identity and Cellular Interactions of Nanoparticles

Alexandre Albanese,[†,‡,▽] Carl D. Walkey,[†,‡,▽] Jonathan B. Olsen,[‡,§] Hongbo Guo,[‡,§] Andrew Emili,[‡,§] and Warren C. W. Chan[†,‡,⊥,∥,#,*]

[†]Institute of Biomaterials and Biomedical Engineering, University of Toronto, Toronto, Ontario M5R 0A3, Canada, [‡]Terrence Donnelly Centre for Cellular and Biomolecular Research, University of Toronto, Toronto, Ontario M5R 0A3, Canada, [§]Banting and Best Department of Medical Research, University of Toronto, Toronto, Ontario M5R 0A3, Canada, [⊥]Chemical Engineering and Applied Chemistry, University of Toronto, Toronto, Ontario M5R 0A3, Canada, [∥]Department of Chemistry, University of Toronto, Toronto, Ontario M5R 0A3, Canada, and [#]Materials Science and Engineering, University of Toronto, Toronto, Ontario M5R 0A3, Canada. [▽]A. Albanese and C. D. Walkey contributed equally.

ABSTRACT A nanoparticle's physical and chemical properties at the time of cell contact will determine the ensuing cellular response. Aggregation and the formation of a protein corona in the extracellular environment will alter nanoparticle size, shape, and surface properties, giving it a "biological identity" that is distinct from its initial "synthetic identity". The biological identity of a nanoparticle depends on the composition of the surrounding biological environment and determines subsequent cellular interactions. When studying nanoparticle–cell interactions, previous studies have ignored the dynamic composition of the extracellular environment as cells deplete and secrete biomolecules in a process known as "conditioning". Here, we show that cell conditioning induces gold nanoparticle aggregation and changes the protein corona composition in a manner that depends on nanoparticle diameter, surface chemistry, and cell phenotype. The evolution of the biological identity in conditioned media enhances the cell membrane affinity, uptake, and retention of nanoparticles. These results show that dynamic extracellular environments can alter nanoparticle–cell interactions by modulating the biological identity. The effect of the dynamic nature of biological environments on the biological identity of nanoparticles must be considered to fully understand nano–bio interactions and prevent data misinterpretation.

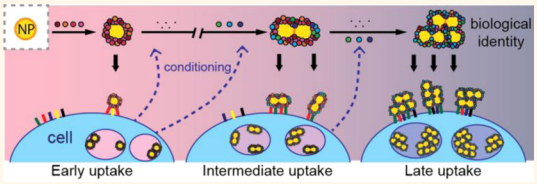

KEYWORDS: nanoparticles · aggregation · protein corona · cell uptake · nano–bio interactions · cell conditioning · biomolecules

Nanoparticles engineered for cellular uptake always interact with the extracellular environment, which contains proteins, lipids, polysaccharides, nucleotides, and ions in the biological medium.[1,2] Interactions between these biomolecules and a nanoparticle often initiate the formation of a "protein corona" that changes the nanoparticle's surface and increases its diameter.[3−5] The transport of nanoparticles through the extracellular environment alters their initial "synthetic identity" and produces a "biological identity" that determines what is "seen" by cell surface receptors.[3,4] The adsorption of proteins onto a nanoparticle affects interactions with the cell membrane by masking the nanoparticle's original surface and promoting the recruitment of various additional receptors. Studies characterizing the protein corona have revealed that its composition depends on the initial properties of the nanoparticle surface, including curvature, charge, and hydrophobicity.[6−8] The protein corona's importance in dictating nanoparticle–cell interactions has led to a growing desire to evaluate how a nanoparticle's design influences its biological identity.

Previous studies have defined the "biological identity" as the nanoparticle plus the adsorbed protein corona.[4,9,10] However, the exposure of nanoparticles to a biological environment can also generate nanoparticle aggregates *via* surface destabilization or protein–protein interactions.[11−15] Aggregation is an important yet overlooked aspect of the biological identity. The transformation of monodisperse nanoparticles into aggregates affects interactions at the nano–bio interface by altering the presentation

* Address correspondence to warren.chan@utoronto.ca.

Received for review November 26, 2013 and accepted May 5, 2014.

Published online May 05, 2014
10.1021/nn4061012

of surface-adsorbed proteins to the cell's receptors.[16] Aggregates are large and require an increased recruitment of cell receptors to drive internalization.[17,18] Aggregates also possess an irregular morphology that produces multiple cell binding configurations with unequal uptake efficiencies.[16,19] When aggregates change the presentation of corona proteins to the cell membrane, this alters nanoparticle–cell interactions and changes the cell response. Thus, characterization of both the protein corona and nanoparticle aggregation in a biological environment is necessary to accurately describe the biological identity of a nanoparticle.

The protein corona has been recognized as a dynamic entity that "evolves" as proteins continuously adsorb to the nanoparticle surface, desorb, and are replaced by other proteins.[3,20] It has been shown that the transfer of nanoparticles from one biological environment into another alters the protein corona composition.[21] The tendency of a protein corona to reflect its surrounding environment demonstrates a certain plasticity to the biological identity. To date, the majority of studies characterizing a nanoparticle's biological identity have used static biological environments such as blood serum, plasma, or cell culture medium. In these environments, nanoparticles reach a steady-state biological identity within minutes to hours. There is an assumption that the biological identity formed in these static biological environments reflects the nanoparticle's properties at the time of cell contact. However, the composition of the extracellular environments is not static. Cells continuously "condition" their microenvironment by changing the concentration of proteins, nutrients, small solutes, and ions.[22,23] The arrival of nanoparticles into the dynamic extracellular environment may change the protein corona, cause aggregation, and alter downstream nanoparticle–cell interactions. The effect of cell conditioning is especially a concern when conducting *in vitro* studies where nanoparticles are incubated with cell populations between 4 and 24 h. Many studies have examined the effect of nanoparticle size, shape, and surface chemistry on cell uptake.[11,24–28] Unfortunately, these studies ignored the dynamic nature of the extracellular environment and the effects of cell conditioning. It remains unknown how the subtle yet progressive conditioning of the extracellular environment affects a nanoparticle's biological identity and subsequent nanoparticle–cell interactions.

The objective of this study is to characterize how conditioning of the cell culture medium influences the biological identity of extracellular nanoparticles. We synthesized different nanoparticles and exposed them to media from cancer cell cultures. We evaluated how progressive cell conditioning affected nanoparticle aggregation and the protein corona using multiple independent techniques. Aggregation was characterized using absorbance spectroscopy, dynamic light scattering, and transmission electron miscroscopy. The protein corona was characterized using polyacrylamide gel electrophoresis (PAGE), quantitative mass spectrometry, and Western blotting. Finally, we investigated how the evolution of the biological identity influences nanoparticle association, uptake, and retention by cells.

RESULTS AND DISCUSSION

Nanoparticle Aggregation in Cultured Media of Different Cell Types. We chose gold nanoparticles as a model system because they can be easily synthesized from 10 to 100 nm with a narrow size distribution and readily functionalized with chemically diverse surface ligands.[29,30] We prepared 15 nm gold nanoparticles and modified them with three different surface ligands: citrate, 11-mercaptoundecanoic acid (MUA), and thiolated poly(ethylene glycol) (PEG) (Table S1, Supporting Information). Citrate coordinates weakly to the gold surface through bidentate carboxylate functional groups, while MUA and PEG form strong coordinate covalent bonds with the gold surface through their terminal thiol functional groups. These ligands mimic some of the surface chemistries that are most common among nanoparticles used in biological applications. Citrate is used as a control nanoparticle surface while MUA and PEG coatings are used to create model anionic and nonfouling surfaces, respectively. After synthesis, the nanoparticles were incubated in phosphate-buffered saline (PBS) supplemented with 10% (v/v) fetal bovine serum (FBS) for 1 h. Nanoparticles were serum pretreated prior to all of our experiments to establish an initial biological identity. This allowed us to then evaluate how subsequent exposure to cells or conditioned media changed the biological identity of nanoparticles.

In our first set of experiments, serum pretreated nanoparticles were incubated with monolayers of A549 lung epithelial carcinoma cells, HeLa cervical carcinoma cells, MDA-MB-435 melanoma cells, or RAW264.7 macrophage-like cells. Aggregation was measured in the isolated culture media using UV–visible spectrophotometry. The degree of aggregation was quantified using an "aggregation index", which is the ratio of the absorbance at 620 nm to the absorbance at 520 nm.[31] The aggregation index quantifies the red shift in the surface plasmon resonance band and correlates with the extent of nanoparticle aggregation.[16] Citrate-coated nanoparticles aggregated to detectable levels within 1 h of exposure to all of the cell types tested (Figure 1a–c and Figure S1, Supporting Information). By 24 h, nanoparticles in contact with A549, HeLa, and RAW264.7 cells had aggregated to a similar extent, whereas nanoparticles exposed to MDA-MB-435 cells were significantly less aggregated. Coating the gold nanoparticles with MUA or PEG significantly decreased aggregation. By 24 h,

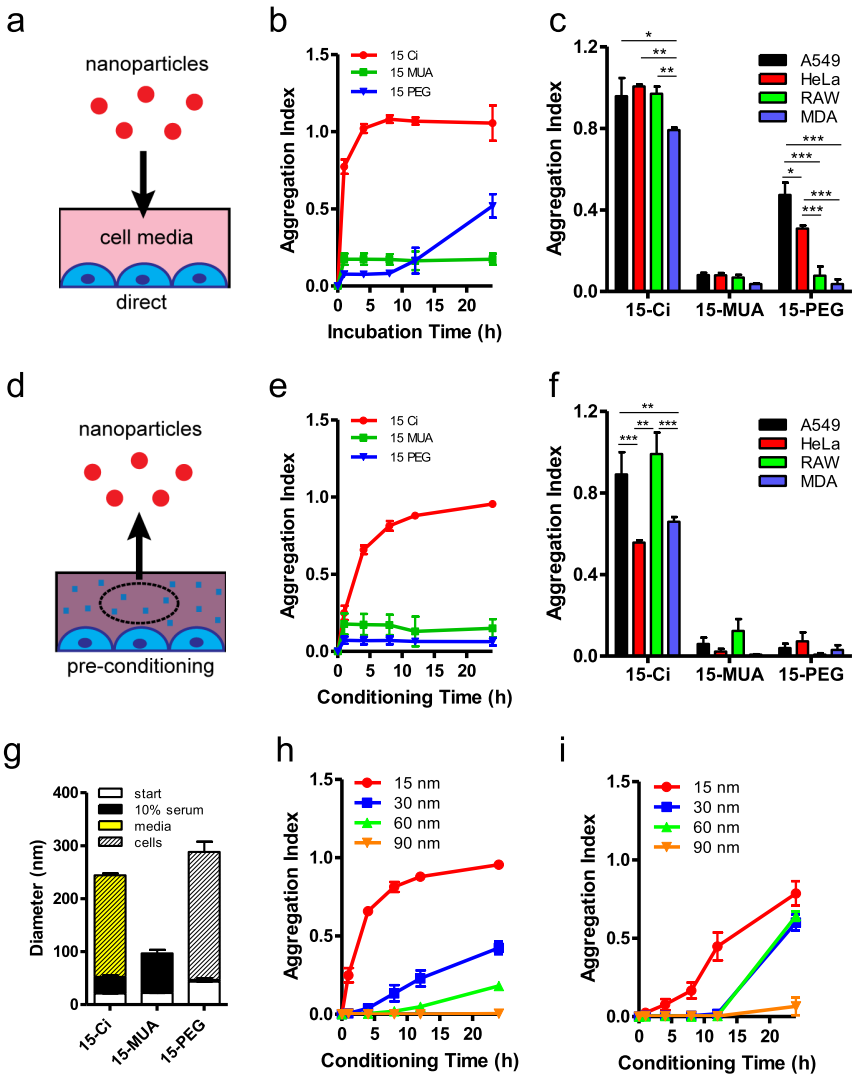

Figure 1. Aggregation of nanoparticles exposed to conditioned media. (a) Scheme of nanoparticles directly exposed to cells. (b) Aggregation index assessed by UV−visible spectrophotometry of nanoparticles directly exposed to A549 cell cultures. (c) Aggregation index after 24 h exposure to various cell lines. (d) Scheme of nanoparticles exposed to cell-conditioned media. (e) Aggregation index of nanoparticles incubated with A549 cell-conditioned media for 4 h. (f) Aggregation index after exposure to 24 h cell-conditioned media for 4 h. (g) Hydrodynamic diameter of nanoparticles exposed to A549 cells or cell-conditioned media. For 15 nm citrate-coated nanoparticles (15-Ci), direct cell exposure and cell conditioning produces the same hydrodynamic diameter (yellow hashed region). For 15 nm PEG-coated nanoparticles (15-PEG), only direct cell exposure causes an increase in hydrodynamic diameter (white hashed region). (h) Aggregation index of citrate-coated nanoparticles possessing different diameters exposed to A549-cell conditioned media for 4 h. (i) Aggregation index of citrate-coated nanoparticles possessing different diameters exposed to RAW 264.7 cell-conditioned media for 4 h. Data presented as the average with standard error from at least three separate experiments.

PEG-coated nanoparticles exposed to A549 and HeLa cells had aggregated slightly, whereas MUA-coated nanoparticles show no difference in aggregation index upon exposure to conditioned media from any cell source. These results show that nanoparticles can aggregate when they are dispersed in culture medium and exposed to cells. The aggregation kinetics depend on nanoparticle surface chemistry and cell phenotype.

We hypothesized that cellular conditioning of the culture medium was responsible for observed nanoparticle aggregation. To test this, conditioned media was collected from A549 cells at time points ranging from 1 to 24 h. To establish optimal incubation time, serum pretreated citrate-coated nanoparticles were transferred into the A549 cell conditioned media and incubated between 0.5 and 8 h at 37 °C in 5% CO_2. Nanoparticle aggregation was proportional to incubation time in the conditioned media and eventually reached a plateau (Figure S2, Supporting Information). We chose a 4 h incubation time with the conditioned media for all of our experiments since this produced an aggregation index that was greater than 75% of the 8 h incubation. Having established our experimental conditions, we proceeded to collect conditioned media from the different cell lines between 1 and 24 h. Serum pretreated citrate, MUA, and PEG nanoparticles

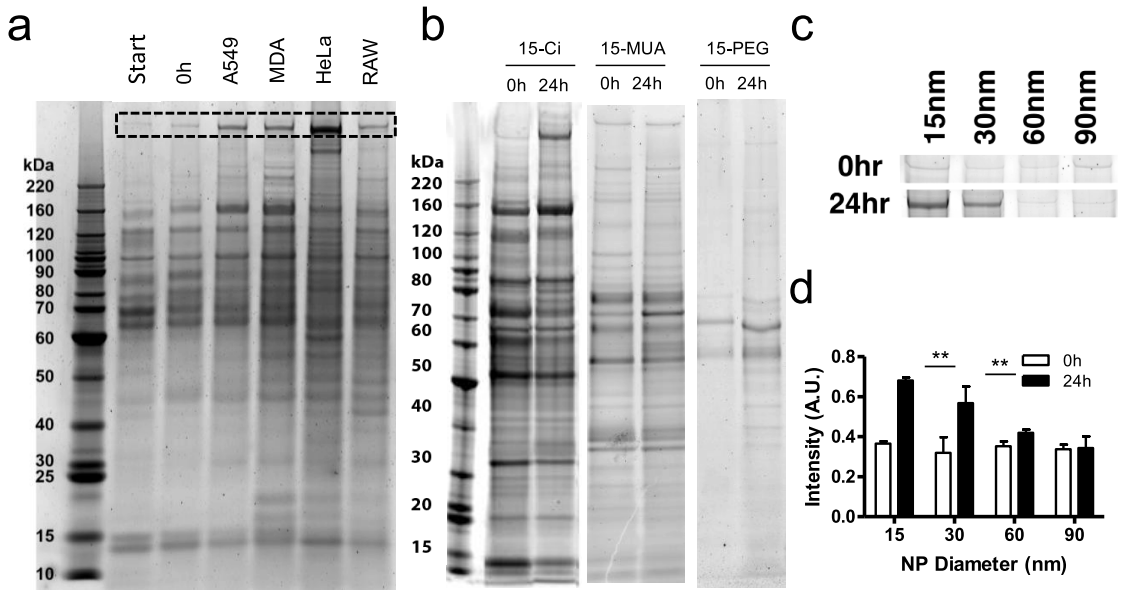

Figure 2. Protein corona of nanoparticles exposed to conditioned media. (a) Krypton stained PAGE gel showing protein corona isolates from 15 nm citrate-coated gold nanoparticles after initial 10% serum exposure (start) and after exposure to fresh (0 h) or 24 h cell-conditioned media for 4 h. Dashed box included to highlight a large (>220 kDa) protein that shows visible change after exposure to conditioned media. (b) Krypton stained PAGE gel of 15 nm citrate-coated (15-Ci), MUA-coated (15-MUA), or PEG-coated (15-PEG) gold nanoparticles exposed to fresh or 24 h A549 conditioned media for 4 h. Images (c) and densitometry (d) of >220 kDa protein band when different nanoparticle sizes were exposed to 24 h A549 cell-conditioned medium. ($n = 3$; ** $p < 0.01$ using two-way ANOVA).

were exposed to the various conditioned media for 4 h and analyzed by absorbance spectrophotometry (Figure 1d–f). Citrate-coated nanoparticles aggregated during incubation with the conditioned media from all cell lines; however, the rate of aggregation was significantly lower than the direct contact of nanoparticles with cells (Figure S3, Supporting Information). By 24 h, citrate-coated nanoparticles in media conditioned by A549 and RAW264.7 cells had aggregated to the same extent as citrate-coated nanoparticles in direct contact with cells (Figure 1f). In contrast, citrate-coated nanoparticles incubated with media conditioned by MDA-MB-435 and HeLa cells aggregated significantly less than nanoparticles in direct contact with cells (Figure 1e,f). PEG-coated nanoparticles did not aggregate in conditioned media, suggesting that their mechanism of aggregation requires direct cell contact. Additional experiments varying the cell number and media volume used to prepare the conditioned media confirmed that nanoparticle aggregation kinetics were related to the rate of media conditioning (Figure S4, Supporting Information). We used dynamic light scattering and electron microscopy as complementary techniques to validate absorbance spectroscopy data and to confirm the presence of aggregates in samples with high aggregation index values (Figure 1g, Figure S5 and Table S1, Supporting Information).

Previous studies have shown that nanoparticle surface curvature influences nanoparticle aggregation kinetics and protein–nanoparticle interactions.[8,32–34] To investigate the effect of nanoparticle diameter on nanoparticle aggregation in conditioned media, we synthesized 30, 60, and 90 nm citrate-coated gold nanoparticles and exposed them to A549 or RAW264.7 cell conditioned media (Table S1, Supporting Information). In both media, smaller nanoparticles aggregated more quickly and to a greater extent than larger nanoparticles (Figure 1h,i and Figures S6 and S7, Supporting Information). Together, these results show that nanoparticles exposed to conditioned media can aggregate over time, suggesting that medium conditioning is at least partially responsible for nanoparticle aggregation during cell exposure. Furthermore, the results demonstrate that nanoparticle size and surface chemistry, cell phenotype, and media conditioning time are important factors influencing the aggregation kinetics.

Protein Corona Composition in Conditioned Media. We investigated the effect of media conditioning on the composition of the protein corona. Serum pretreated 15 nm citrate-coated nanoparticles were transferred to unconditioned media or media that had been conditioned by A549, MDA-MB-435, HeLa, or RAW264.7 cells for 24 h. Nanoparticles were incubated in the media for 4 h, purified, and washed to remove unbound proteins. Adsorbed proteins were then isolated from the nanoparticles and characterized using polyacrylamide gel electrophoresis (PAGE) (Figure 2a). PAGE analysis shows that exposing the nanoparticles to conditioned media leads to qualitative changes in the composition of the protein corona, in a manner that depended on the phenotype of the cells that conditioned the media (Figure 2a). However, all cell lines produced a visible

increase in the abundance of a high molecular weight (>220 kDa) band. Additional experiments revealed that the abundance of this protein correlates with media conditioning time (Figure S8, Supporting Information). These results show that the protein corona around citrate-coated nanoparticles is altered by conditioned culture medium in a manner that depends on conditioning time and cell phenotype.

We also characterized the composition of the protein corona around MUA- and PEG-coated nanoparticles after exposure to conditioned media. In unconditioned media, far less protein adsorbed to PEG-coated nanoparticles relative to citrate-coated nanoparticles (Figure 2b and Figure S9, Supporting Information). After exposure to A549 cell-conditioned media, the total quantity of adsorbed protein increased on the PEG-coated nanoparticles. In unconditioned media, proteins adsorbed to MUA-coated nanoparticles to a similar extent as citrate-coated nanoparticles. However, during exposure to conditioned media, the composition of the protein corona around MUA-modified gold nanoparticles did not change in A549 cell-conditioned media. These results establish that nanoparticle surface chemistry influences the stability of the protein corona composition in conditioned media.

To understand the influence of nanoparticle size on protein corona stability, we characterized the evolution of the protein corona around 30, 60, and 90 nm citrate-coated nanoparticles in A549 cell-conditioned media (Figure S10, Supporting Information). Incubation in conditioned media led to the appearance of the characteristic high molecular weight (>220 kDa) band for all nanoparticle sizes tested (Figure 2c,d). However, the intensity of the band was inversely proportional to nanoparticle diameter (Figure 2d) and correlated with the extent of nanoparticle aggregation (Figure 1h). These results show that protein corona composition is altered upon exposure to conditioned media, which depends on nanoparticle size and surface curvature. Smaller nanoparticles underwent a greater change in protein corona composition than larger nanoparticles. This may be due to the greater deflection angle between adjacent adsorbed proteins, which makes the underlying gold surface more accessible to incoming biomolecules and increases the protein exchange rate. Exposing the nanoparticles to RAW264.7 cell-conditioned media also produced size-dependent changes in the band pattern that were qualitatively different from the changes observed in A549 cell-conditioned media (Figure S11, Supporting Information), revealing that cell phenotype contributes to size-dependent trends in protein corona compositional changes.

To gain a more detailed understanding of protein corona composition in conditioned media, we used liquid chromatography–tandem mass spectrometry (LC–MS/MS) to characterize changes in the composition of the protein corona formed around 15 nm citrate-coated nanoparticles during incubation with media conditioned by A549 cells.[6,33] A total of 581 proteins were identified, of which 113 were sufficiently abundant to allow accurate quantification by spectral counting. The protein corona formed after 1, 8, and 24 h of conditioning is 89, 84, and 81% similar to the corona formed after exposure to unconditioned media, respectively. The relative abundance of each identified protein was influenced in a different way by media conditioning. Proteins with similar trends were divided into six groups by unsupervised hierarchical clustering (Figure 3a). The combined relative abundance of group 3 proteins decreased from ~40% (w/w) in unconditioned medium to ~20% (w/w) in medium that had been conditioned for 24 h. In contrast, the combined relative abundance of group 4 proteins increases from ~20% (w/w) in unconditioned media to ~40% (w/w) in medium that has been conditioned for 24 h. These results suggest that group 4 proteins gradually replace group 3 proteins as cells condition the nanoparticle's surrounding medium. The five most abundant group 3 proteins are vitronectin, thrombin, plasma serum protease inhibitor, complement C3, and coagulation factor V, while the five most abundant group 4 proteins are thrombospondin, antithrombin III, apolipoprotein B, talin, and myosin (Table S2, Supporting Information). LC–MS/MS data illustrates that the protein corona around nanoparticles is altered in conditioned media.

FBS supplies the proteins in unconditioned media, whereas both FBS and human-derived A549 cells supply the proteins in conditioned media. Species-specific differences (human *vs* bovine) in the protein-derived peptides sequenced by LC–MS/MS allow us to assign the origin of each identified protein to either FBS or A549 cells. The relative abundance of cell-derived proteins in the corona gradually increases as the culture media is conditioned. By 24 h, cell-derived proteins account for at least 4.8% (w/w) of the total adsorbed protein mass. The relative abundance of human fibronectin increases in proportion to media conditioning time, although the total amount of adsorbed fibronectin stays roughly constant (Figure 3b). This trend was confirmed by Western blotting using an antihuman-fibronectin antibody (Figure 3c). The appearance of human-derived fibronectin in the corona correlates with the secretion of this protein into the culture medium by the cells (Figure S12, Supporting Information). Similar trends were observed for myosin and thrombospondin by LC–MS/MS quantification. Overall, these results suggest that cell-secreted proteins progressively replace serum-derived proteins in the protein corona around citrate-coated nanoparticles as the culture medium is conditioned.

Aggregation Mechanism. The time-dependent compositional changes in the protein corona of citrate-coated

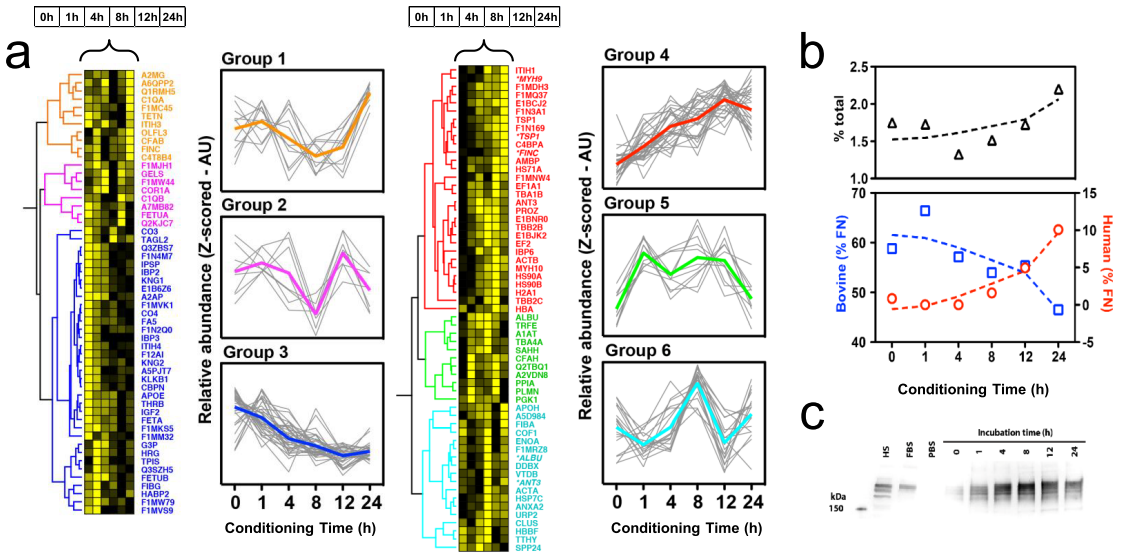

Figure 3. Quantitative analysis of the protein corona formed around gold nanoparticles exposed to conditioned media. (a) Heat map showing abundance of 113 proteins identified within the protein corona of 15 nm citrate-coated gold nanoparticles exposed to a conditioned media. Proteins were identified using liquid chromatography−tandem mass spectrometry (LC−MS/MS) and quantified by spectral counting. Each row corresponds to a protein, and each column corresponds to the duration of culture medium conditioning by A549 cells. Abbreviated protein names are explained in Table S2 (Supporting Information). The intensity of the yellow color is related to the relative abundance (by mass) of a given protein within the protein corona. Relative abundances were mean-centered and variance-scaled (Z-scored) across conditioning times. Proteins were clustered into six groups based on correlations in their relative abundance across medium conditioning times. A dendrogram is presented on the left of the heat map outlining protein grouping. The relative abundance trend for each protein in each group is displayed on the right of the heat map. The bold colored line is the average for each group. (b) Top panel: Total fibronectin (as a fraction of total adsorbed protein mass) as a function of medium conditioning time. Bottom panel: Proportion of adsorbed fibronectin derived from fetal bovine serum (left axis: blue) or human A549 cells (right axis: red). Relative abundances were estimated by spectral counting. (c) Western blot of protein corona isolates from 15 nm citrate-coated gold nanoparticles exposed to A549 cell-conditioned media. Blots were probed using an antihuman fibronectin antibody. Control wells contain human serum (HS) as a positive control, fetal bovine serum (FBS), and phosphate-buffered saline (PBS) as negative controls.

nanoparticles correlates with aggregation in conditioned media (Figure 1e *vs* Figure 3c). This suggests that the accumulation of cell-secreted proteins such as fibronectin, thrombospondin, or myosin in the protein corona may cause nanoparticle aggregation. To determine whether cellular proteins are responsible for nanoparticle aggregation, we filtered conditioned media through a 10 kDa membrane to separate low molecular weight components from the proteins. PAGE analysis confirmed that there were no detectable protein bands in the low molecular weight filtrate, while the protein composition in the high molecular weight retentate is similar to whole media (Figure 4a). We then characterized the aggregation of 15 nm citrate-coated nanoparticles in whole media, the protein-free filtrate, and the protein-rich retentate (Figure 4b,c). The fractionation of unconditioned medium did not produce any detectable nanoparticle aggregation. For conditioned media, we were surprised to find that exposure to the protein-free filtrate caused significant aggregation, while the protein-containing retentate did not (two-way ANOVA, $p < 0.001$). The extent to which the protein-free filtrate induced nanoparticle aggregation depended on the cell type used to condition the medium. The filtrate from A549 cell conditioned media caused significantly more aggregation than whole media suggesting that the presence of proteins may slightly reduce aggregation (two-way ANOVA, $p < 0.001$). For RAW264.7 cells, whole conditioned media or its protein-free filtrate caused a similar degree of nanoparticle aggregation (two-way ANOVA, $p < 0.001$). Although the time-dependent accumulation of sub-10 kDa components in the conditioned media causes the progressive aggregation of nanoparticles in both cell lines, our data demonstrates that aggregation kinetics and mechanism may be cell-line dependent. It is likely that the mechanism of aggregation (secreted biomolecules *vs* secreted proteins) will vary depending on nanoparticle composition and surface chemistry. Our findings demonstrate that in the absence of serum and cell-secreted proteins, low molecular weight components such as ions, biological molecules, and metabolites can cause the aggregation of serum-pretreated 15 nm citrate-stabilized nanoparticles.

Effect of Media Conditioning on Nanoparticle Cell Uptake. Next, we investigated how changes in the biological identity of nanoparticles affected cell uptake. Previous studies have demonstrated that aggregation and modulation of the protein corona can influence the cellular

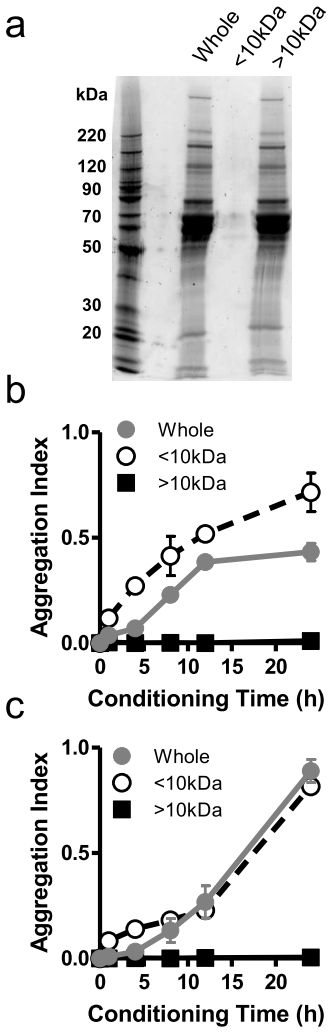

Figure 4. Filtration of the conditioned media. (a) Krypton stained PAGE gel demonstrating the protein content of whole medium, protein-depleted <10 kDa filtrate and protein-rich >10 kDa retentate fractionated using a 10 kDa Amicon centrifuge filter. Aggregation index of 15 nm citrate-coated nanoparticles exposed to media, filtrate and retentate of A549 (b) or RAW 264.7 (c) cell conditioned media. Data represents the mean and standard error of three independent experiments.

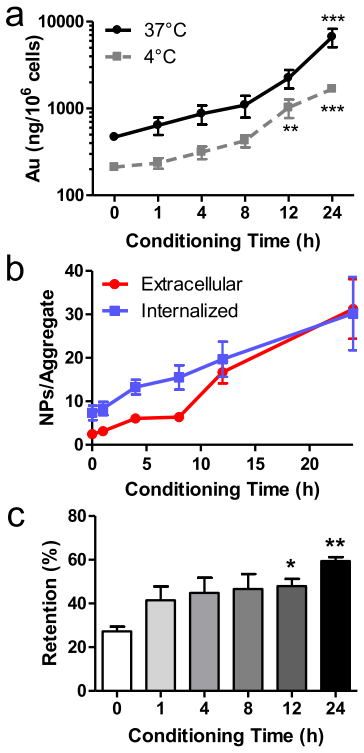

Figure 5. Cell uptake of nanoparticles exposed to conditioned media. (a) ICP-AES-based cell uptake measurement of 15 nm citrate-coated nanoparticles exposed to A549 conditioned media between 1 and 24 h. Nanoparticles were incubated with cells for 1 h at 37 or 4 °C. Data represents the mean and standard error from three independent experiments. $^{**}p < 0.01$, $^{***}p < 0.001$ using two-way ANOVA. (b) Average size of nanoparticle aggregates exposed to A549 cells (extracellular) and imaged in the intracellular vesicles (internalized) after 1 h incubation with cells. Data was obtained by analysis of electron microscope images. (c) Retention of membrane-bound 15 nm citrate-coated nanoparticles incubated for 1 h at 4 °C, washed, and incubated at 37 °C for 4 h. Data represents the mean and standard error from three independent experiments; $^{*}p < 0.05$, $^{**}p < 0.01$, using ANOVA.

interactions of nanoparticles.[6,16,35−37] We incubated 15 nm citrate-coated nanoparticles with media that had been conditioned for 0 to 24 h and characterized association with A549 cells using inductively coupled plasma-atomic emission spectroscopy (ICP-AES) (Figure 5a). The results reveal that exposure to conditioned media enhances the nanoparticle−cell association of citrate-coated nanoparticles. Since elemental analysis cannot distinguish between internalized and membrane-bound nanoparticles, we used electron microscopy (EM) to characterize the cellular distribution of the nanoparticles. The majority of the nanoparticles observed by EM were located within intracellular vesicles, showing that cell-associated nanoparticles were mostly internalized (Figure S13, Supporting Information). EM reveals that monodisperse nanoparticles prepared in fresh media (0 h) appear as small aggregates inside cellular vesicles (Figure 5b). Our observations are consistent with previous studies reporting the formation of nanoparticle aggregates subsequent to cell uptake.[24,25,38] For nanoparticles exposed to conditioned media, the formation of aggregates prior to cell contact (Figure 1e and Figure S5, Supporting Information) caused an overall increase in the size of intracellular aggregates (Figure 5b). The size of both extracellular and intracellular aggregates increases as a function of time-dependent cell conditioning. Cell association experiments performed at 4 °C reveal that exposure to conditioned media increases the binding avidity of nanoparticles to the cell membrane (Figure 5a). Once bound to the cell membrane, nanoparticles exposed to conditioned media had significantly higher cell retention (Figure 5c). Together, these findings show that cell conditioning of the extracellular environment changes the biological identity of citrate-coated 15 nm nanoparticles and promotes the cell

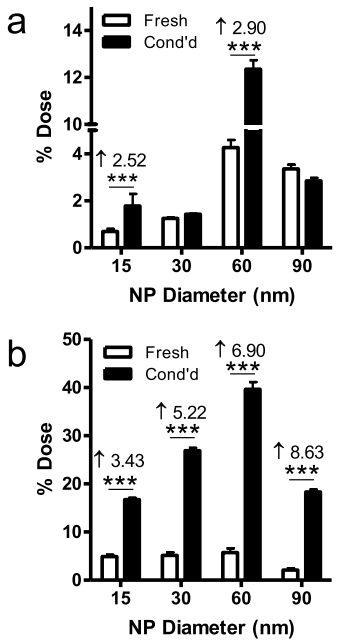

Figure 6. Effect of conditioned media on size-dependent uptake. (a) A549 cell uptake of 15, 30, 60, and 90 nm citrate-coated nanoparticles exposed to fresh or 24 h A549 cell-conditioned media (cond'd). (b) RAW 264.7 cell uptake of 15, 30, 60, and 90 nm citrate-coated nanoparticles exposed to fresh or 24 h RAW264.7 cell-conditioned media. Cells were incubated with nanoparticles for 1 h at 37 °C, and uptake was quantified using ICP-AES. Numbers indicate the fold increase in uptake of conditioned media exposed nanoparticles relative to their counterparts in fresh medium. Comparisons were performed at 0 and 24 h using ANOVA where *** $p < 0.001$.

uptake of larger nanoparticle aggregates. We suspect that the increased cell membrane affinity, uptake, and retention of the nanoparticles are due to the combined effect of large aggregate size and the presence of cell-derived proteins within the corona. Because of their larger size, aggregates are likely to bind more receptors than monodisperse nanoparticles[16,17] and display decreased exocytosis rates.[25] The incorporation of cell-secreted proteins into the corona may also increase receptor affinity or target additional receptors. The exposure of 15 nm citrate-coated nanoparticles to conditioned media leads to the incorporation of thrombospondin and cellular fibronectin into the protein corona. It is possible that progressive accumulation of these proteins, which are involved in cell−cell and cell-matrix interactions, allows nanoparticles to bind highly expressed cell-surface receptors.

Our studies demonstrate that a nanoparticle's biological identity evolves in extracellular environment as a result of cell conditioning. By overlooking the effect of cell conditioning on nanoparticle−cell interactions, it is possible to misinterpret experimental data. We explored how this oversight could potentially affect data interpretation by investigating the effect of cell conditioning on the size-dependent uptake of citrate-coated nanoparticles in nonphagocytic A549 cells and phagocytic RAW 264.7 cells. A549 cells preferentially internalized 60 nm nanoparticles in both unconditioned and conditioned media (Figure 6a). In unconditioned media, the uptake of 60 nm nanoparticles was ~2.5 times higher than 30 nm nanoparticles, whereas in conditioned media, the uptake of the 60 nm nanoparticles rose to nearly 8 times that of the 30 nm nanoparticles. RAW264.7 cells internalized citrate-coated nanoparticles of all sizes to similar extents in unconditioned media (Figure 6b). However, in conditioned media, RAW264.7 cells preferentially internalized 60 nm nanoparticles. Experiments with these cell lines reveal that conditioned media produces design-specific changes in nonphagocytic nanoparticle uptake and an overall increase in nanoparticle phagocytosis. These results show that size-dependent uptake trends can vary based on the composition of the extracellular environment. In the presence of metabolically active cells, nanoparticles are exposed to dynamic extracellular environments that can alter their biological identity. In cell culture experiments, the evolution of the medium's composition will depend on cell numbers, cell phenotype, medium volume, and incubation time. Slight changes to the experimental conditions will change the rate of cell conditioning and directly influence nanoparticle uptake trends. The overlooked influence of cell conditioning may explain the apparent inconsistencies in nanoparticle uptake studies.[33,39−41]

CONCLUSION

This study establishes that cell conditioning of the extracellular environment can alter the biological identity of a nanoparticle and change its cell uptake (Figure 7). Upon exposure to a biological environment, a nanoparticle will acquire an initial biological identity that results in a specific rate of cell uptake. The secretion of cell-derived proteins and metabolites alters the extracellular environment and can lead to nanoparticle aggregation and changes to the protein corona. These changes in the nanoparticle's biological identity will alter the rate and mechanism of cell uptake. How cell conditioning influences the nanoparticle's biological identity depends on its size and surface chemistry, as well as the cell's phenotype and culture conditions. The dynamic evolution of the extracellular environment and its impact on the nanoparticle's biological identity should be considered during *in vitro* experiments to fully explain nanoparticle−cell interactions. Researchers should characterize the biological identity of a nanoparticle in unconditioned and conditioned media in future experiments. This will provide a better characterization of a nanoparticle's "true" biological identity prior to cell contact, strengthen conclusions made about the effect of nanoparticle physical and chemical properties on nanoparticle−cell interactions, and prevent data misinterpretation.

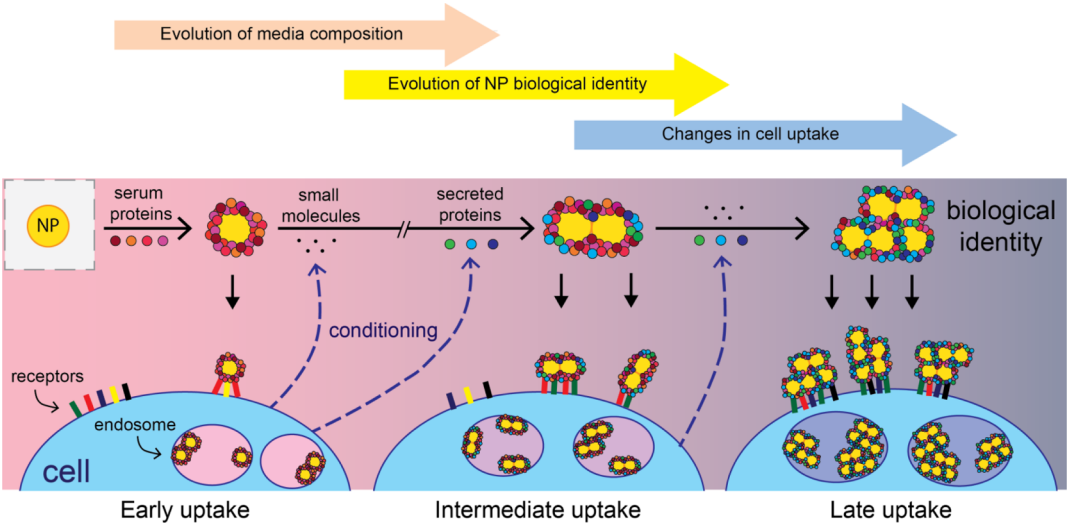

Figure 7. Evolution of nanoparticles in the extracellular environment. The figure demonstrates how initial exposure of the nanoparticle to a biological environment creates an initial biological identity through the formation of a protein corona or nanoparticle aggregation. Cell secretion of metabolites and proteins leads to changes in the protein corona and nanoparticle aggregation. As the biological identity of nanoparticles evolves over time so does receptor binding, receptor recruitment, and cell uptake. This model was based on our data from the serum pretreated 15 nm citrate-coated nanoparticles. Of note, the rate by which the cell changes the nanoparticle's biological identity is likely to depend on the particle surface chemistry, size or shape, and cell type.

Our findings also bring into question the mechanisms of nanoparticle uptake. In previous studies we proposed that single and monodisperse nanoparticles form aggregates at the cell membrane as a result of receptor clustering.[24,25,42] Receptor clustering is required to generate enough potential energy for membrane wrapping and internalization of the nanoparticles.[18,24] We proposed that nanoparticle aggregation at the cell surface may be necessary for the active endocytosis of small nanoparticles. Results from the current study reveal an alternative explanation for the appearance of nanoparticle aggregates on the cell membrane and inside intracellular vesicles. In the membrane-wrapping hypothesis, monodisperse nanoparticles aggregate *via* receptor clustering at the cell membrane. Our current study suggests an additional "preaggregation" model where the arrival of nanoparticles into the extracellular region adjacent to the cell membrane leads to interactions with secreted biomolecules. In this model, nanoparticle aggregation occurs prior to contact with the cell surface membrane. The aggregated nanoparticles will engage more cell-surface receptors and generate more potential energy for membrane wrapping than their dispersed counterparts. The contributions of "preaggregation" and "receptor clustering" are likely dependent on a nanoparticle's design, cell type, and composition of the extracellular environment. Future empirical and mathematical studies will be necessary to determine the respective contributions of each mechanism during cell uptake.

Our study also raises questions about how the dynamic nature of biological environments *in vivo* will impact nanoparticle–cell interactions. Although biological environments work to maintain homeostasis, they are subject to continuous compositional fluctuations. The composition of plasma, interstitial fluid, mucus, and saliva can change in response to metabolism, inflammation, and disease.[43–46] When nanoparticles are introduced into the body, they may initially appear as a monodisperse population with well-characterized surface chemistries. However, circulation through the body may lead to adsorption of a protein corona and nanoparticle aggregation over time. Our study was designed to investigate how time-dependent changes in the extracellular environment affected nanoparticle properties. Time-dependent changes are unlikely to be as remarkable *in vivo*. Instead, nanoparticles will be subjected to different environments *via* translocation from the blood into various tissues. In the tissue, biomolecules secreted by multiple cell types and the composition of the protein-dense extracellular matrix will generate unique microenvironments. The results suggest that the biological identity of blood-borne nanoparticles is likely to be altered in each of these microenvironments. Our study also suggests that the formation of aggregates in the blood or within a tissue's microenvironment may lead to increased phagocytosis (Figure 6b). Aggregates may also cause a decrease in tissue accumulation due to size-restricted transport through the vasculature and the extracellular matrix.[47,48] The dynamic nature of extracellular environments and the numerous unique microenvironments inside the body may generate multiple biological identities and ultimately influence blood clearance trends, biodistribution patterns, and

therapeutic efficiencies. This study provides the first evidence of the extracellular environment's effect on nanoparticle aggregation, protein corona composition, and cellular interactions. A cell's ability to indirectly modify a nanoparticle through the secretion of biomolecules reveals an overlooked interaction occurring at the nano–bio interface and highlights the underestimated complexity of nanoparticle–cell interactions. This study contributes to an ongoing effort to characterize nano–bio interactions in order to establish guidelines for the design of effective nanomaterials.[7,48]

METHODS

Nanoparticle Preparation. The 15 nm gold nanoparticles were prepared by citrate reduction according to the Frens–Turkovich method.[49] Nanoparticles were then modified with thiol-terminated methoxyPEG-5000 or 11-mercaptoundecanoic acid (MUA) using standard ligand-exchange procedures.[30] The 15 nm nanoparticles were also used as seeds for the preparation of 30, 60, and 90 nm gold nanoparticles by hydroquinone-mediated growth.[29] The nanoparticles were synthesized, washed three times *via* centrifugation with 0.01% (w/v) sodium citrate tribasic, and incubated in PBS containing 10% (v/v) fetal bovine serum (FBS) for 1 h at 37 °C. The nanoparticles were centrifuged and added to cells or preconditioned media at 5 nM (3×10^{12} nanoparticles/mL) for 15 nm nanoparticles. Larger nanoparticle concentrations were normalized to achieve the same surface area as the 15 nm nanoparticles (2.1×10^{15} nm^2/mL).

Cell Experiments. Cell experiments were conducted with A549 human lung epithelial carcinoma cells, HeLa human cervix epithelial adenocarcinoma cells, RAW 264.7 murine leukemia virus-transformed monocyte cells, and MDA-MB-435 human melanocyte cells. Nanoparticle experiments were conducted in phenol-free DMEM (Life Technologies) containing 25 mM HEPES and supplemented with 10% FBS (Sigma) and penicillin-streptomycin (Life Technologies). 12-well plates were seeded with 8×10^5 MDA-MB-435 or HeLa cells, 1.6×10^5 RAW 264.7 cells, or 3×10^5 A549 cells to achieve 85% confluency. 835 μL of media was added to cells and incubated for 1 to 24 h. When using other types of culture plates, such as 48-well or 6-well, we normalized cell numbers and media volume to the growth surface's area to maintain identical cell-to-media ratios. For direct cell exposure experiments, nanoparticles were diluted in phenol-free DMEM + 10% FBS prior to experiment and directly added to cells for 1, 4, 8, 12, and 24 h. Conditioned media was generated by adding phenol-free DMEM + 10% FBS to all cell lines and collected at 1, 4, 8, 12, and 24 h. For conditioned media experiments, nanoparticles were incubated with preconditioned media for 4 h at 37 °C. A 4 h incubation time between nanoparticles and conditioned media was chosen on the basis of preliminary experiments demonstrating that nanoparticle aggregation reached a plateau between 4 and 8 h.

Characterization of Nanoparticle Aggregation. After exposure to cells or preconditioned media, nanoparticles were kept on ice and analyzed by UV–visible spectrometry (Shimadzu) to assess aggregation by quantification of the plasmonic red-shift. We used the 620/520, 620/527, 700/544, and 700/577 nm absorbance ratios as the "aggregation index" for 15, 30, 60, and 90 nm nanoparticles, respectively. Aggregation index values were subtracted by the aggregation index of nanoparticles in fresh medium. When comparing the aggregation of 15 nm nanoparticles in various cell cultures and supernatants, we determined the rate of aggregation using the following hyperbolic equation:

$$y = y_{max}(1 - e^{-kx})$$

where y is the aggregation index (620/520 nm), y_{max} is the maximum aggregation index at 24 h, x is time in hours, and k is the aggregation rate. Conditions were set to $y_{max} < 1.2$ since this is the maximum possible value using our experimental conditions. All points were fit to the equation producing fits at $R^2 > 0.88$. The curves of individual replicate series were obtained and compared to other conditions to determine statistical differences using ANOVA. Some nanoparticle samples were also analyzed by dynamic light scattering (Malvern) to measure the hydrodynamic diameter and by transmission electron microscopy to measure the size of aggregates. Electron microscope images were analyzed using an ImageJ macro to quantify the number of nanoparticles per aggregate, as previously described.[16]

Characterization of the Protein Corona. After incubation in serum-containing media, gold nanoparticles were purified from unbound protein by repeated centrifugation and resuspension in phosphate buffered saline. Bound protein was stripped by incubating nanoparticles in 2% (w/v) sodium dodecyl sulfate (SDS) and 100 mM dithiothreitol for 1 h at 70 °C. An aliquot of the protein isolates was drawn and resolved on a NuPAGE 4–12% Bis-Tris poly(acrylamide) gel (Invitrogen) in MOPS running buffer (Invitrogen) according to the manufacturer's protocol. The gels were stained using Krypton fluorescent protein stain (Pierce) and imaged on a Typhoon laser scanner (Amersham). For LC–MS/MS, protein isolates were repeatedly precipitated to remove SDS, as described previously.[33] Protein pellets were reduced and alkylated before being digested with trypsin. Protein digests were analyzed on the Orbitrap Velos (Thermo) as described previously.[33] The percentage (w/w) relative abundance of each of each identified protein was estimated using the following formula:

$$RA(n)_{\%(w/w)} = \frac{SpC(n)}{\sum_{i=1}^{m} SpC(i)}$$

where $RA(n)_{\%(w/w)}$ is the relative abundance of protein n, and m is the total number of identified proteins. $SpC(i)$ is the total number of spectral counts recorded for protein i.

Western Blot. Protein corona isolates were run on NuPAGE gels and transferred onto nitrocellulose membrane. The membrane was blocked with 5% milk in 1X PBST for 1 h at room temperature, rinsed, and probed overnight with rabbit antifibronectin (Abcam) in 1X Superblock in PBS (Pierce). The membrane was washed to remove excess primary antibody and probed with horseradish peroxidase-conjugated goat antirabbit (Cell Signaling) in 1X Superblock in PBS for 1 h at room temperature. Membrane was washed to remove unbound secondary antibody and exposed to a chemiluminescence substrate. The membrane was visualized using a CCD camera (Kodak).

Cell Uptake. Cells were prepared the day before by seeding 12-well plates with 3×10^5 A549 cells or 1.67×10^5 RAW264.7 cells overnight. Each cell type was seeded in numbers to achieve 85% confluency at the start of experiment. The 15 nm citrate nanoparticles were exposed to A549 cell-conditioned media for 4 h and then added to A549 cells and incubated for 1 h at 37 °C for uptake studies, for 1 h at 4 °C for membrane binding studies, and for 1 h at 4 °C followed by 4 h in fresh media at 37 °C for retention studies. For experiments with larger nanoparticles, nanoparticle formulations were exposed to either A549 cell-conditioned media for 4 h and then incubated with A549 cells for 1 h at 37 °C or exposed to RAW264.7 cell-conditioned media for 4 h and then incubated with RAW264.7 cells for 1 h at 37 °C. After incubation with nanoparticles, cells were washed three times with PBS + 0.5% bovine serum albumin and frozen until elemental analysis. Samples were thawed, digested with 0.5 mL of nitric acid for 30 min at 70 °C, diluted in 3 mL of Millipure water, and analyzed by ICP-AES. Samples were analyzed for Au and Mg content. The Mg content

was used to quantify the number of cells per sample in reference to cell standards.[50] The ICP-AES data was converted to obtain gold quantification as ng/cell and multiplied by the average number of RAW264.7 or A549 cells in a given experiment (to minimize variability caused by differences in cell number). The nanoparticle exposure dose was determined by measuring an aliquot of nanoparticles by ICP-AES. The percentage dose was defined as

$$[\text{ng of gold in all cells}] \div [\text{ng of nanoparticles added}] \times 100\%$$

Conflict of Interest: The authors declare no competing financial interest.

Acknowledgment. This work was supported by the Natural Sciences and Engineering Research Council of Canada (NSERC) (NETGP35015, BIOPSYS Network RGPIN-288231), Canadian Institute of Health Research (COP-126588 and MOP-93532), Canadian Health Research Program (CHRJ385829 and CPG-104290), and Canadian Research Chair (950-223824). A.A. was supported by the Ontario Graduate Scholarship. C.D.W. was supported by an NSERC scholarship.

Supporting Information Available: Additional Figures S1–S13 and Tables S1 and S2. This material is available free of charge *via* the Internet at http://pubs.acs.org.

REFERENCES AND NOTES

1. Stark, W. J. Nanoparticles in Biological Systems. *Angew. Chem., Int. Ed.* **2011**, *50*, 1242–1258.
2. Nel, A. E.; Madler, L.; Velegol, D.; Xia, T.; Hoek, E. M.; Somasundaran, P.; Klaessig, F.; Castranova, V.; Thompson, M. Understanding Biophysicochemical Interactions at the Nano–Bio Interface. *Nat. Mater.* **2009**, *8*, 543–557.
3. Walkey, C. D.; Chan, W. C. Understanding and Controlling the Interaction of Nanomaterials with Proteins in a Physiological Environment. *Chem. Soc. Rev.* **2012**, *41*, 2780–2799.
4. Monopoli, M. P.; Aberg, C.; Salvati, A.; Dawson, K. A. Biomolecular Coronas Provide the Biological Identity of Nanosized Materials. *Nat. Nanotechnol.* **2012**, *7*, 779–786.
5. Tenzer, S.; Docter, D.; Kuharev, J.; Musyanovych, A.; Fetz, V.; Hecht, R.; Schlenk, F.; Fischer, D.; Kiouptsi, K.; Reinhardt, C.; *et al.* Rapid Formation of Plasma Protein Corona Critically Affects Nanoparticle Pathophysiology. *Nat. Nanotechnol.* **2013**, *8*, 772–781.
6. Tenzer, S.; Docter, D.; Rosfa, S.; Wlodarski, A.; Kuharev, J.; Rekik, A.; Knauer, S. K.; Bantz, C.; Nawroth, T.; Bier, C.; *et al.* Nanoparticle Size Is a Critical Physicochemical Determinant of the Human Blood Plasma Corona: A Comprehensive Quantitative Proteomic Analysis. *ACS Nano* **2011**, *5*, 7155–7167.
7. Walkey, C. D.; Olsen, J. B.; Song, F.; Liu, R.; Guo, H.; Olsen, D. W.; Cohen, Y.; Emili, A.; Chan, W. C. Protein Corona Fingerprinting Predicts the Cellular Interaction of Gold and Silver Nanoparticles. *ACS Nano* **2014**, *8*, 2439–2455.
8. Lundqvist, M.; Stigler, J.; Elia, G.; Lynch, I.; Cedervall, T.; Dawson, K. A. Nanoparticle Size and Surface Properties Determine the Protein Corona with Possible Implications for Biological Impacts. *Proc. Natl. Acad. Sci. U. S. A.* **2008**, *105*, 14265–14270.
9. Cedervall, T.; Lynch, I.; Lindman, S.; Berggard, T.; Thulin, E.; Nilsson, H.; Dawson, K. A.; Linse, S. Understanding the Nanoparticle–Protein Corona Using Methods to Quantify Exchange Rates and Affinities of Proteins for Nanoparticles. *Proc. Natl. Acad. Sci. U. S. A.* **2007**, *104*, 2050–2055.
10. Lynch, I.; Cedervall, T.; Lundqvist, M.; Cabaleiro-Lago, C.; Linse, S.; Dawson, K. A. The Nanoparticle-Protein Complex as a Biological Entity; A Complex Fluids and Surface Science Challenge for the 21st Century. *Adv. Colloid Interface Sci.* **2007**, *134–35*, 167–174.
11. Qiu, Y.; Liu, Y.; Wang, L. M.; Xu, L. G.; Bai, R.; Ji, Y. L.; Wu, X. C.; Zhao, Y. L.; Li, Y. F.; Chen, C. Y. Surface Chemistry and Aspect Ratio Mediated Cellular Uptake of Au Nanorods. *Biomaterials* **2010**, *31*, 7606–7619.
12. Lacerda, S. H.; Park, J. J.; Meuse, C.; Pristinski, D.; Becker, M. L.; Karim, A.; Douglas, J. F. Interaction of Gold Nanoparticles with Common Human Blood Proteins. *ACS Nano* **2009**, *4*, 365–379.
13. Rausch, K.; Reuter, A.; Fischer, K.; Schmidt, M. Evaluation of Nanoparticle Aggregation in Human Blood Serum. *Biomacromolecules* **2010**, *11*, 2836–2839.
14. Maiorano, G.; Sabella, S.; Sorce, B.; Brunetti, V.; Malvindi, M. A.; Cingolani, R.; Pompa, P. P. Effects of Cell Culture Media on the Dynamic Formation of Protein-Nanoparticle Complexes and Influence on the Cellular Response. *ACS Nano* **2011**, *4*, 7481–7491.
15. Kim, D.; El-Shall, H.; Dennis, D.; Morey, T. Interaction of PLGA Nanoparticles with Human Blood Constituents. *Colloids Surf., B* **2005**, *40*, 83–91.
16. Albanese, A.; Chan, W. C. W. Effect of Gold Nanoparticle Aggregation on Cell Uptake and Toxicity. *ACS Nano* **2011**, *5*, 5478–5489.
17. Yuan, H. Y.; Li, J.; Bao, G.; Zhang, S. L. Variable Nanoparticle-Cell Adhesion Strength Regulates Cellular Uptake. *Phys. Rev. Lett.* **2010**, *105*, 1381011–1381014.
18. Gao, H.; Shi, W.; Freund, L. B. Mechanics of Receptor-Mediated Endocytosis. *Proc. Natl. Acad. Sci. U. S. A.* **2005**, *102*, 9469–2474.
19. Dasgupta, S.; Auth, T.; Gompper, G. Shape and Orientation Matter for the Cellular Uptake of Nonspherical Particles. *Nano Lett.* **2014**, *14*, 687–693.
20. Casals, E.; Pfaller, T.; Duschl, A.; Oostingh, G. J.; Puntes, V. Time Evolution of the Nanoparticle Protein Corona. *ACS Nano* **2010**, *4*, 3623–3632.
21. Lundqvist, M.; Stigler, J.; Cedervall, T.; Berggard, T.; Flanagan, M. B.; Lynch, I.; Elia, G.; Dawson, K. The Evolution of the Protein Corona around Nanoparticles: A Test Study. *ACS Nano* **2011**, *5*, 7503–7509.
22. Kulasingam, V.; Diamandis, E. P. Proteomics Analysis of Conditioned Media from Three Breast Cancer Cell Lines: A Mine for Biomarkers and Therapeutic Targets. *Mol. Cell Proteomics* **2007**, *6*, 1997–2011.
23. Skalnikova, H.; Motlik, J.; Gadher, S. J.; Kovarova, H. Mapping of the Secretome of Primary Isolates of Mammalian Cells, Stem Cells and Derived Cell Lines. *Proteomics* **2011**, *11*, 691–708.
24. Chithrani, B. D.; Ghazani, A. A.; Chan, W. C. Determining the Size and Shape Dependence of Gold Nanoparticle Uptake into Mammalian Cells. *Nano Lett.* **2006**, *6*, 662–668.
25. Chithrani, B. D.; Chan, W. C. Elucidating the Mechanism of Cellular Uptake and Removal of Protein-Coated Gold Nanoparticles of Different Sizes and Shapes. *Nano Lett.* **2007**, *7*, 1542–1550.
26. Clift, M. J.; Rothen-Rutishauser, B.; Brown, D. M.; Duffin, R.; Donaldson, K.; Proudfoot, L.; Guy, K.; Stone, V. The Impact of Different Nanoparticle Surface Chemistry and Size on Uptake and Toxicity in a Murine Macrophage Cell Line. *Toxicol. Appl. Pharmacol.* **2008**, *232*, 418–427.
27. Pan, Y.; Neuss, S.; Leifert, A.; Fischler, M.; Wen, F.; Simon, U.; Schmid, G.; Brandau, W.; Jahnen-Dechent, W. Size-Dependent Cytotoxicity of Gold Nanoparticles. *Small* **2007**, *3*, 1941–1949.
28. Hauck, T. S.; Ghazani, A. A.; Chan, W. C. Assessing the Effect of Surface Chemistry on Gold Nanorod Uptake, Toxicity, and Gene Expression in Mammalian Cells. *Small* **2008**, *4*, 153–159.
29. Perrault, S. D.; Chan, W. C. W. Synthesis and Surface Modification of Highly Monodispersed, Spherical Gold Nanoparticles of 50–200 nm. *J. Am. Chem. Soc.* **2009**, *131*, 17042–17043.
30. Lin, S.-Y.; Tsai, Y.-T.; Chen, C.-C.; Lin, C.-M.; Chen, C.-h. Two-Step Functionalization of Neutral and Positively Charged Thiols onto Citrate-Stabilized Au Nanoparticles. *J. Phys. Chem. B* **2004**, *108*, 2134–2139.
31. Guan, J.; Li, J.; Guo, Y.; Yang, W. S. Cooperative Dual-Stimuli-Triggered Aggregation of Poly-L-Histidine-Functionalized Au Nanoparticles. *Langmuir* **2009**, *25*, 2679–2683.
32. Roach, P.; Farrar, D.; Perry, C. C. Surface Tailoring for Controlled Protein Adsorption: Effect of Topography at

the Nanometer Scale and Chemistry. *J. Am. Chem. Soc.* **2006**, *128*, 3939–3945.
33. Walkey, C. D.; Olsen, J. B.; Guo, H.; Emili, A.; Chan, W. C. Nanoparticle Size and Surface Chemistry Determine Serum Protein Adsorption and Macrophage Uptake. *J. Am. Chem. Soc.* **2012**, *134*, 2139–2147.
34. Schaefer, B.; Hecht, M.; Harting, J.; Nirschl, H. Agglomeration and Filtration of Colloidal Suspensions with DVLO Interactions in Simulation and Experiment. *J. Colloid Interface Sci.* **2010**, *349*, 186–195.
35. Lesniak, A.; Campbell, A.; Monopoli, M. P.; Lynch, I.; Salvati, A.; Dawson, K. A. Serum Heat Inactivation Affects Protein Corona Composition and Nanoparticle Uptake. *Biomaterials* **2010**, *31*, 9511–9518.
36. Lesniak, A.; Fenaroli, F.; Monopoli, M. R.; Aberg, C.; Dawson, K. A.; Salvati, A. Effects of the Presence or Absence of a Protein Corona on Silica Nanoparticle Uptake and Impact on Cells. *ACS Nano* **2012**, *6*, 5845–5857.
37. Limbach, L. K.; Li, Y. C.; Grass, R. N.; Brunner, T. J.; Hintermann, M. A.; Muller, M.; Gunther, D.; Stark, W. J. Oxide Nanoparticle Uptake in Human Lung Fibroblasts: Effects of Particle Size, Agglomeration, and Diffusion at Low Concentrations. *Environ. Sci. Technol.* **2005**, *39*, 9370–9376.
38. Kneipp, J.; Kneipp, H.; Rice, W. L.; Kneipp, K. Optical Probes for Biological Applications Based on Surface-Enhanced Raman Scattering from Indocyanine Green on Gold Nanoparticles. *Anal. Chem.* **2005**, *77*, 2381–2385.
39. Levy, R.; Shaheen, U.; Cesbron, Y.; See, V. Gold Nanoparticles Delivery in Mammalian Live Cells: a Critical Review. *Nano Rev.* **2010**, *1*, 1–18.
40. Xu, A.; Yao, M.; Xu, G.; Ying, J.; Ma, W.; Li, B.; Jin, Y. A Physical Model for the Size-Dependent Cellular Uptake of Nanoparticles Modified with Cationic Surfactants. *Int. J. Nanomedicine* **2012**, *7*, 3547–3554.
41. Oh, W. K.; Kim, S.; Choi, M.; Kim, C.; Jeong, Y. S.; Cho, B. R.; Hahn, J. S.; Jang, J. Cellular Uptake, Cytotoxicity, and Innate Immune Response of Silica-Titania Hollow Nanoparticles Based on Size and Surface Functionality. *ACS Nano* **2010**, *4*, 5301–5313.
42. Jiang, W.; Kim, B. Y.; Rutka, J. T.; Chan, W. C. Nanoparticle-Mediated Cellular Response is Size-Dependent. *Nat. Nanotechnol.* **2008**, *3*, 145–150.
43. Touitou, Y.; Touitou, C.; Bogdan, A.; Reinberg, A.; Auzeby, A.; Beck, H.; Guillet, P. Differences Between Young and Elderly Subjects in Seasonal and Circadian Variations of Total Plasma Proteins and Blood Volume as Reflected by Hemoglobin, Hematocrit, and Erythrocyte Counts. *Clin. Chem.* **1986**, *32*, 801–804.
44. Shub, M. D.; Pang, K. Y.; Swann, D. A.; Walker, W. A. Age-Related Changes in Chemical Composition and Physical Properties of Mucus Glycoproteins from Rat Small intestine. *Biochem. J.* **1983**, *215*, 405–411.
45. Dawes, C. Circadian Rhythms in Human Salivary Flow Rate and Composition. *J. Physiol.* **1972**, *220*, 529–545.
46. Bates, D.; Levick, J.; Mortimer, P. Change in Macro Molecular Composition of Interstitial Fluid from Swollen Arms after Breast Cancer Treatment, and Its Implications. *Clin. Sci.* **1993**, *85*, 737–746.
47. Perrault, S. D.; Walkey, C.; Jennings, T.; Fischer, H. C.; Chan, W. C. Mediating Tumor Targeting Efficiency of Nanoparticles Through Design. *Nano Lett.* **2009**, *9*, 1909–1915.
48. Albanese, A.; Lam, A. K.; Sykes, E. A.; Rocheleau, J. V.; Chan, W. C. Tumour-on-a-Chip Provides an Optical Window into Nanoparticle Tissue Transport. *Nat. Commun.* **2013**, *4*, 2718.
49. Frens, G. Controlled Nucleation for Regulation of Particle-Size in Monodisperse Gold Suspensions. *Nature (London), Phys. Sci.* **1973**, *241*, 20–22.
50. Albanese, A.; Tsoi, K. M.; Chan, W. C. Simultaneous Quantification of Cells and Nanomaterials by Inductive-Coupled Plasma Techniques. *J. Lab. Autom.* **2012**, *18*, 99–104.